

An idealized physical model for the severe convective storm environmental sounding

Submitted to Journal of the Atmospheric Sciences, under review

DANIEL R. CHAVAS*

Purdue University, Department of Earth, Atmospheric, and Planetary Sciences, West Lafayette, IN

DANIEL T. DAWSON II

Purdue

ABSTRACT

A recent study proposed a novel physical model for the transient thermodynamic environment favorable for severe convective storms based on the vertical structure of dry and moist static energy. From this foundation, this work develops a model for steady thermodynamic and kinematic profiles for severe convective storm environments. The model physics are described and an algorithm presented to apply the model to generate a sounding for numerical simulations of severe convective storms. The theoretical sounding is fit to a case-study sounding associated with the 3 May 1999 tornado outbreak, and its potential utility is demonstrated via idealized numerical simulation experiments. A long-lived supercell is successfully simulated with the original sounding but not the analogous theoretical sounding. Two types of example experiments are then performed that do simulate a long-lived supercell: 1) a semi-theoretical experiment in which a portion of the theoretical sounding is modified to match the real sounding (low-level moisture); 2) a fully theoretical experiment in which a model physical parameter is varied (free-tropospheric relative humidity). Overall, the construction of this minimal model is flexible and amenable to additional modifications as needed. The model offers a novel framework that can be used to test sensitivities of severe convective storms to the vertical structure of the environment and to link this structural variability to the physical processes that produce them within the climate system.

1. Introduction

While substantial advances have been made in the understanding and prediction of severe convective storms (SCS), operational predictability remains limited and thus substantial risks to life and property persist. From 1995–2015, tornadoes caused 1710 deaths in the U.S., ranking as third-deadliest weather phenomenon (NOAA). Our ability to predict these weather risks in the current or future climate depends crucially on a physical understanding of the dependence of SCS events on their larger-scale environment. However, our understanding of this dependence has largely focused on bulk thermodynamic and kinematic parameters that intrinsically mask variability in the *vertical structure* of the thermodynamic and kinematic profiles. This leads to a simple question: what details within a particular sounding actually matter for the evolution of a severe convective storm? This lack of knowledge limits our ability to predict SCS events and their risks both operationally and on climate timescales.

SCS research focuses principally on supercells, which produce the majority of SCS-related hazardous weather, particularly significant tornadoes (Duda and Gallus 2013). Past work has demonstrated that supercells are associated with large magnitudes of CAPE and 0–6km bulk vertical wind shear (Weisman and Klemp 1982a, 1984a; Tippett et al. 2015); the product of the two constitutes an environmental proxy for potential SCS activity (Brooks et al. 2003; Gensini and Ashley 2011; Seeley and Roms 2015). Significant tornado events are further linked to high magnitudes of low-level storm-relative environmental helicity (SREH) and low values of the lifting condensation level (LCL) (Brooks et al. 1994; Rasmussen and Blanchard 1998; Thompson et al. 2003, 2004). This suite of environmental bulk parameters are now widely employed as part of an “ingredients-based” framework for modern weather forecasting of the spatial distribution of severe thunderstorm and tornado risk (Doswell III et al. 1996; Doswell 2001; Tippett et al. 2015). This approach can also provide meaningful insight into the spatial and temporal distribution of SCS activity in the U.S. (Gensini and Ashley 2011), including long-term spatial shifts in tornado activity (Agee et al. 2016; Gensini and Brooks 2018). Moreover, these bulk parameter proxies have been used to esti-

*Corresponding author address: Daniel R. Chavas, Purdue University, Department of Earth, Atmospheric, and Planetary Sciences, 550 Stadium Mall Drive HAMP 3221, West Lafayette, IN 47907.
E-mail: drchavas@gmail.com

mate changes in severe weather and tornado risk under future climate change (Trapp et al. 2007, 2009; Diffenbaugh et al. 2013; Seeley and Roms 2015).

However, the use of bulk quantities reflects a gap in our fundamental physical understanding of how severe convective storms and tornadoes emerge from, and evolve within, a given background environment. These bulk quantities are by definition vertically-integrated measures of the environment, and thus two environments can yield the same bulk value despite having very different vertical thermodynamic and kinematic structures (McCaul Jr and Weisman 2001). Yet the effects of higher-order vertical variability on the probabilities of specific modes of convective organization as well as tornadogenesis remains poorly understood. This lack of understanding is likely an important contributor to low SCS predictability on daily and sub-daily time scale (e.g. Elmore et al. 2002a,b; Cintineo and Stensrud 2013). Moreover, bulk proxy statistical relationships trained on canonical high CAPE and high bulk shear environments may be inappropriately applied to non-canonical environments, such as ones with high bulk shear yet relatively low CAPE in which quasi-linear convective systems are common (Sherburn and Parker 2014). Finally, because bulk proxies are necessarily validated only against a relatively short historical record, their application to future climates is not only uncertain but potentially misleading if the chosen proxies do not correctly scale with actual SCS risk across climate states (Trapp et al. 2011; Gensini and Mote 2015; Hoogewind et al. 2017; Trapp and Hoogewind 2016; Trapp et al. 2019). The above issues indicate the need for a deeper physical understanding of the role of the vertical thermodynamic and kinematic structure for fixed values of a given bulk proxy.

Weisman and Klemp (1984) (hereafter WK84) were among the first to investigate how SCS morphology and evolution depend on vertical environmental structure (Weisman and Klemp 1982b, 1984b). They used a 3D cloud-system-resolving numerical model (CRM) initialized with a range of horizontally homogeneous environments specified by analytical functions for the vertical thermodynamic and kinematic profiles. From this work emerged the WK84 parametric thermodynamic and kinematic profiles, which have since been used in numerous idealized CRM studies to investigate many different aspects of SCS and their environments. This includes three categories of experiments: 1) parameter sweep studies varying CAPE and shear (Lawson 2019); 2) the vertical distribution of buoyancy or shear at fixed values of CAPE and bulk shear, respectively (McCaul Jr and Weisman 2001; Kirkpatrick et al. 2009; Guarriello et al. 2018; Brown and Nowotarski 2019); and 3) variations in parameters independent of bulk quantities, particularly free-tropospheric moisture (Gilmore and Wicker 1998; James and Markowski 2010; McCaul and Cohen 2004; Honda and Kawano 2015). This seminal work using parametric

sounding models to test sensitivities of convective evolution at fixed CAPE represents the foundation that we seek to build off of for this study.

While the WK84 sounding has been undeniably useful in advancing our understanding of basic storm dynamics over the past few decades, its construction is somewhat ad hoc – its structure and intrinsic variability is purely parametric rather than physical in nature. An ideal alternative is a model for the environmental sounding that is defined by the physics of how these environments are generated in the first place within the climate system. Recently, Agard and Emanuel (2017, hereafter AE17) developed the first theoretical model for the time-dependent 1-dimensional vertical thermodynamic state associated with severe weather environments. This state represents the archetypal conceptual model of the generation of transient high-CAPE environments over eastern North America (Carlson and Ludlam 1968; Benjamin and Carlson 1986; Benjamin 1986; Doswell 2001). A schematic of this set-up is provided in Figure 1, in which warm moist low-level air from the Gulf of Mexico is advected northward, undercutting dry well-mixed air that is advected eastward off the elevated terrain to the west. AE17 used this model to demonstrate analytically how transient peak CAPE may increase with climate change.

In principle, the AE17 theoretical model could be used to specify a steady environmental sounding for use in numerical simulation experiments. This could further allow tests of fundamental SCS sensitivities to the external physical parameters that specify the model environment while holding bulk parameters (e.g. CAPE) fixed. However, this model has yet to be phrased in a way that it can directly define a sounding for use in an idealized CRM, nor has it been applied in SCS numerical simulations, real-world or idealized. Thus, there is a significant opportunity to apply this physical model for the thermodynamic environment to modern SCS numerical modeling experiments. Doing so would allow careful testing of how SCS evolution depends on key physical parameters in the vertical thermodynamic structure. These parameters could eventually be linked to climate-scale processes to understand how climate variability influences not only CAPE and bulk shear but also those parameters that define the vertical thermodynamic structure for a given bulk parameter value. Such physical linkages from climate to mesoscale to storm-scale are critical for understanding both fundamental SCS thermodynamic sensitivities as well as how SCS activity may change in a future climate.

To fill this gap, this work seeks to extend AE17 to develop a novel theoretical model for a complete, steady SCS environmental (thermodynamic + kinematic) sounding for use in numerical simulation experiments. The present work focuses on how our model is constructed and provide an illustrative example of how it can be used as a theoretical foundation for both observationally motivated sensi-

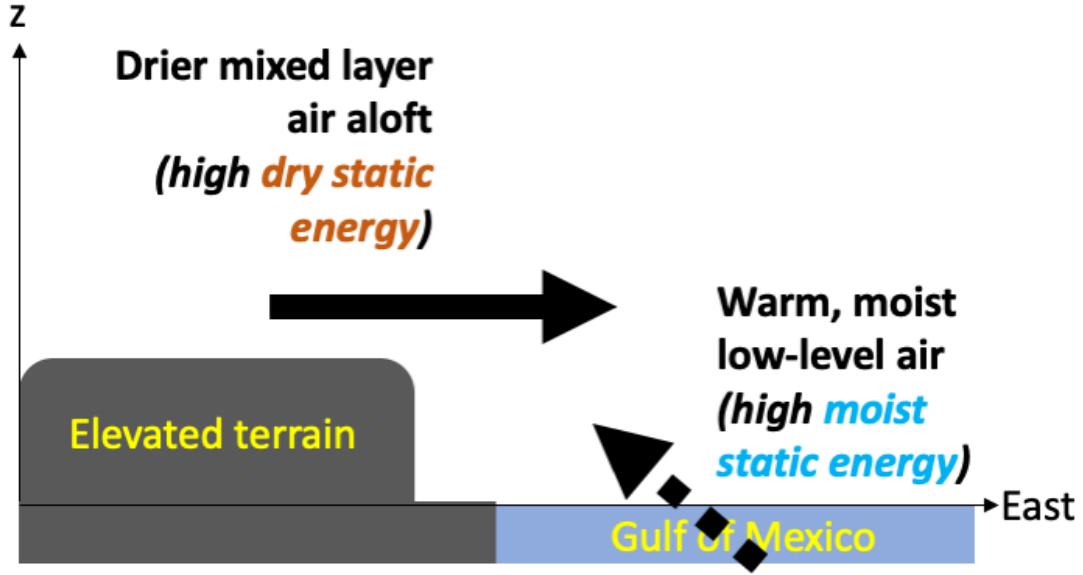


FIG. 1: Conceptual diagram of how an environment with large CAPE is generated over Eastern North America, in a static energy framework following Agard and Emanuel (2017).

tivity testing and controlled experimentation. Thus, the specific outcomes of our simulation examples shown here are *not* intended to demonstrate robust sensitivities. Moreover, the way we apply our model is by no means the only approach, it is simply a relatively straightforward one. We hope that as the model is put into use in future research it may evolve further, or perhaps it will be applied in different ways for different types of experiments. These types of comprehensive experimentation and in-depth analysis are left for future work.

Our methodology is described in Section 2. Section 3 explains how the theoretical model is constructed. Section 4 provides an example application of how our model can be fit to a sounding from a historical tornado outbreak and a demonstration of the potential experimental utility of the model using high-resolution numerical simulation experiments. Discussion and conclusions are provided in Section 5.

2. Methodology

a. Overview

We first develop the theoretical model. We then fit the model to a sounding associated with an observed SCS event: a proximity sounding from a simulation of the 3 May 1999 tornado outbreak (Dawson et al. 2010), which was the largest outbreak in Oklahoma history and produced multiple supercells and long-track tornadoes (Speheger et al. 2002). Finally, we demonstrate the model’s potential experimental utility via illustrative sensitivity tests

of variability in vertical structure at fixed bulk CAPE and shear.

b. Numerical model description

Experiments are performed using the CM1 model (Bryan and Fritsch 2002) version 19. CM1 is a fully compressible nonhydrostatic numerical model designed for idealized simulations of mesoscale and smaller atmospheric phenomena. CM1 has been employed to gain fundamental insight into a wide range of mesoscale phenomena in both the mid-latitudes and tropics, including severe convective storms and tornadoes (Bryan et al. 2006; James and Markowski 2010; Naylor and Gilmore 2012; Orf et al. 2017; Dahl et al. 2012, 2014; Naylor and Gilmore 2014; Parker 2014; Dahl 2015; Markowski 2016), supercells (James and Markowski 2010; Coffey and Parker 2015; Davenport and Parker 2015; Nowotarski and Markowski 2016) and convective squall lines (Bryan et al. 2006); tropical cyclones (Bryan and Rotunno 2009; Chavas and Emanuel 2014; Davis 2015; Navarro and Hakim 2016; Naylor and Schechter 2014; Bu et al. 2014; Peng et al. 2018); and the scaling of vertical velocity, precipitation extremes, and CAPE with climate in radiative-convective equilibrium (Singh and O’Gorman 2013, 2014, 2015).

CM1 is particularly well-suited for this work for a number of reasons, including 1) it has demonstrated flexibility across a range of scales and scientific questions; 2) its excellent mass and momentum conservation properties; and 3) inclusion of various thermodynamic terms often neglected in other models (such as the heat capacity of

hydrometeors), which may be important on convection-resolving scales. Moreover, CM1 uses a height-based vertical coordinate, which fits naturally with our static energy-based theoretical sounding framework.

c. Experiments

The setup of the simulation domain, grid parameters, and physical parameterizations closely follows that of Dawson et al. (2019). Each of our simulation experiments is performed on a $200 \times 200 \times 20 \text{ km}^3$ domain with a horizontal grid spacing of 250 m in an inner $100 \times 100 \text{ km}^2$ region and gradually stretched to 1 km at the lateral boundaries. The lateral boundary conditions are open radiative, while the top and bottom boundaries are impermeable and free-slip. A Rayleigh damping layer is located above 15 km with an inverse e-folding time of $1/300 \text{ s}^{-1}$. The vertical grid has 50 levels stretched from 20 m at the surface to $\sim 800 \text{ m}$ at the model top (20 km). The domain translates with a constant $[\mathbf{u}, \mathbf{v}] = [7.28, 8.78] \text{ m s}^{-1}$ to keep the simulated storm near the center of the domain. Deep convection is initiated using the Naylor and Gilmore (2012) updraft nudging technique applied to an ellipsoidal region with maximum $w = 10 \text{ m s}^{-1}$ and radii $10 \text{ km} \times 10 \text{ km} \times 1.5 \text{ km}$ and centered at $[x, y, z] = [100, 100, 1.5] \text{ km}$ over the first 900 s of model integration. The NSSL triple-moment microphysics scheme (Mansell 2010; Dawson et al. 2014) and a 1.5-order prognostic TKE turbulence closure scheme (Deardorff 1980) is used. Finally, as is common in idealized CRM simulations of deep convection, no radiation or surface physics are included. All simulations are run for 4 h. We perform simulation experiments using four soundings described in Table 1 to define the horizontally homogeneous initial environment.

Our example historical event (3MAY99) is a proximity sounding from a simulation of the 3 May 1999 tornado outbreak, from Dawson et al. (2010). We then perform simulations with our model fit to 3MAY99 (THEO; fitting described in Section 4a). Finally, we perform two experiments to illustrate distinct uses of the model: 1) experiment using a semi-theoretical sounding that tests the inclusion of specific details of the real sounding (here: low-level moisture) into the theoretical model (MODHIST), and 2) experiment using a fully-theoretical sounding that tests direct modifications of theoretical model parameters (here: free-tropospheric relative humidity; MODTHEO).

3. Theoretical model for SCS environmental sounding

a. Foundation: AE17 model

The AE17 model provides a useful foundation for generating physics-based environments with high CAPE amenable to SCS numerical simulation experiments.

Name	Details
3MAY99 (Historical)	Proximity sounding from a simulation of the 3 May 1999 tornado outbreak, from Dawson et al. (2010)
THEO	Pure theoretical model fit to 3MAY99
MODHIST	THEO with the low-level moisture set equal to values from 3MAY99 historical event sounding
MODTHEO	THEO with enhanced constant free tropospheric relative humidity

TABLE 1: Soundings for our experiments.

Specifically, AE17 defines this environment with a time-dependent two-layer model for dry and moist static energies. Neglecting liquid/solid phases of water, moist static energy per unit mass M is given by:

$$M = C_p T + L_v r + gz \quad (1)$$

where T is temperature, r is the water vapor mixing ratio, and z is geopotential height. The quantities C_p , L_v , and g are the specific heat of air, the latent heat of vaporization, and the acceleration due to gravity, respectively, and all may be approximated as constants. Hence, moist static energy is a linear combination of temperature (sensible heat), moisture (latent heat), and altitude (potential energy). Dry static energy, D , is the same as M but taking $r = 0$, i.e.

$$D = C_p T + gz \quad (2)$$

The AE17 model defines a thermodynamic state comprised of a free troposphere (FT) layer with constant dry static energy, D_{FT} , overlying a boundary layer (BL) with constant moist static energy, M_{BL} , and depth H_{BL} . As noted in AE17, CAPE scales with the difference between the boundary-layer moist static energy and the dry static energy, $M_{BL} - D_{FT}$. Meanwhile, the difference in dry static energies between the base of the free troposphere and the boundary layer, $D_{FT} - D_{BL}$, represents a capping inversion. The convective inhibition (CIN) thus depends directly on this dry static energy difference; its magnitude also depends on the BL moisture via its control on the LCL. Thus, a key benefit of this model is that CAPE and CIN may be externalized as model parameters. The latter is particularly beneficial as it explicitly incorporates an externally-defined ‘‘cap’’ into the sounding.

b. Why static energy instead of potential temperature?

While static energies are not commonly employed in the severe weather literature, in a hydrostatic atmosphere their vertical structures are dynamically equivalent to that of their potential temperature counterparts. For example, Figure 2a displays a Skew-T plot for an example our 3 May 1999 tornado outbreak sounding. Figure 2b-c compares the vertical profiles of dry and moist static energy

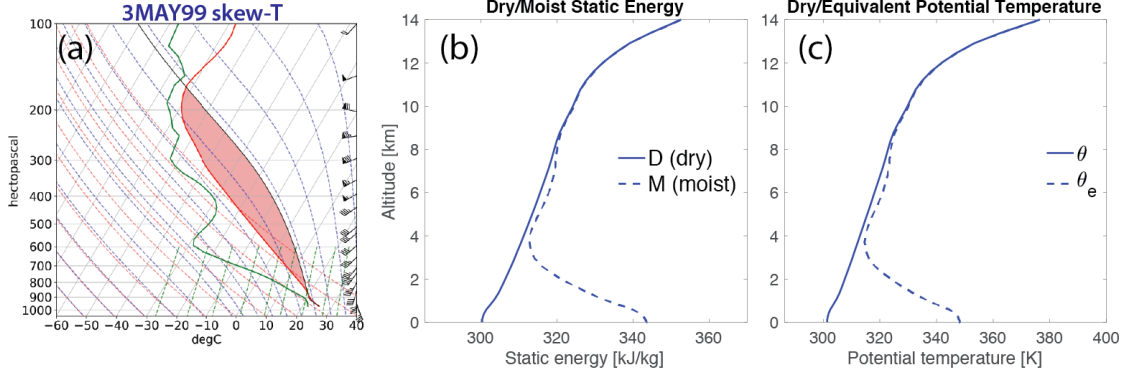


FIG. 2: (a) Skew-T plot for example proximity sounding from historical simulation of the 05/03/99 tornado outbreak at 2300 UTC in SW Oklahoma; (b) vertical profile of dry and moist static energies; (c) vertical profile of dry and equivalent potential temperatures.

and dry and moist (equivalent) potential temperature for our observational case. The absolute values of these two quantities map onto one another non-linearly, but their vertical variations are very similar.

Why do potential temperature and static energy map onto one another in this way? Here we demonstrate their relationship for the dry case; the logic extends to the moist case but is significantly more complicated analytically (Emanuel 2004; Bryan 2008; Roms 2015). We begin from the First Law of Thermodynamics for an ideal gas, given by

$$C_p dT = \dot{q} + \alpha dP \quad (3)$$

where \dot{q} is an external specific heating rate, $\alpha = \frac{1}{\rho}$ is the specific volume, and P is air pressure. We then consider an adiabatic process (such as an air parcel ascending through an atmospheric column): $\dot{q} = 0$. This yields

$$C_p dT = \alpha dP \quad (4)$$

From Eq. (4), dry static energy requires making the assumption of hydrostatic balance,

$$\alpha \frac{dP}{dz} = -g \quad (5)$$

Rearranging this equation and substituting into Eq. (4) gives

$$C_p dT = -g dz \quad (6)$$

which can be written as the conservation equation

$$dD = 0 \quad (7)$$

where D is the dry static energy (Eq. (2))¹. Thus, hydrostatic balance allows us to trade changes in pressure (i.e. pressure-volume work at constant pressure) with changes in altitude (i.e. potential energy).

¹Note that Eq. (6) is readily rearranged to give the dry adiabatic lapse rate, which thus should formally be the “dry adiabatic hydrostatic lapse rate”.

Meanwhile, from Eq. (4), potential temperature requires no new assumption. Instead, we reapply the Ideal Gas Law, $P = \rho R_d T$, where R_d is the specific gas constant for dry air. Rearranging this and plugging in gives

$$C_p d(\ln T) = R_d d(\ln P) \quad (8)$$

which can be written as the conservation equation

$$ds_d = 0 \quad (9)$$

where

$$s_d = C_p \ln T - R_d \ln P \quad (10)$$

is the dry entropy. Adding the constant $R_d \ln P_0$, where P_0 is a reference pressure, to both sides and rearranging yields

$$s_d + R_d \ln P_0 = C_p \ln \theta \quad (11)$$

where

$$\theta = T \left(\frac{P_0}{P} \right)^{\frac{R_d}{C_p}} \quad (12)$$

is the dry potential temperature. We can write θ as

$$\theta = e^{\frac{s_d + R_d \ln P_0}{C_p}} \quad (13)$$

Thus, potential temperature is an alternative, non-linear way to write entropy, in which entropy is modified by constants and then exponentiated.

How are adiabatic changes in dry entropy and dry static energy related? We start from the conservation of s_d (Eq. (10)) since this requires less stringent assumptions. We write the conservation of D (Eq. (2)) as $C_p dT = dD - g dz$ and substitute to yield

$$ds_d = \frac{1}{T} (dD - g dz) - \frac{R_d}{P} dP \quad (14)$$

Reapplying hydrostatic balance, written as $-\frac{R_d}{P} dP = \frac{g}{T} dz$, gives

$$ds_d = \frac{dD}{T} \quad (15)$$

For hydrostatic displacements, incremental changes in entropy are simply given by incremental changes in static energy, divided by temperature. This follows from the basic thermodynamic relationship among entropy, energy, and temperature. Hence, vertical structures of entropy and static energy are qualitatively similar but differ quantitatively owing to variations in temperature with altitude. Finally, we may link D to θ via Eq. (11) to give

$$d(\ln\theta) = \frac{ds_d}{C_p} = \frac{dD}{C_p T} \quad (16)$$

Thus, changes in the natural logarithm of dry potential temperature are related to changes in dry static energy, normalized by the sensible heat of the parcel.

Eq. (16) does not seem especially intuitive, which is the point: while potential temperature is practically useful for translating entropy to a tangible temperature-like quantity, it does so by adding non-linearity to the problem that makes it harder to work with analytically. Moreover, while entropy is better conserved for non-hydrostatic displacements of an air parcel and hence is more precise for defining properties of a lifted parcel relative to its environment (Romps 2015), this more detailed accounting is not necessary for defining a hydrostatically-balanced state.

Thus, the ability to use static energy in lieu of potential temperature for defining a hydrostatic atmospheric profile has significant practical benefits. Given that static energy is a linear sum of three types of energy, it is analytically simple to generate thermodynamic profiles for layers specified by a single value of dry or moist static energy. Moreover, it is straightforward to incorporate additional modifications, including free-tropospheric relative humidity (not specified by the AE17 model), and sub-dry-adiabatic free-tropospheric lapse rates. The latter may be incorporated by allowing for vertical variations in D_{FT} , which may be used to directly vary the vertical distribution of buoyancy associated with a fixed value of CAPE. We aim to exploit these benefits in our work below.

c. Our model

Our goal is to build off of the AE17 framework to develop a model for a complete, steady SCS sounding, i.e. joint thermodynamic and kinematic profiles. As described below, the model represents a transition from predominantly southerly flow advecting warm, moist air near the surface to predominantly westerly flow advecting warm, dry air aloft. In this way, the sounding is physically and intuitively consistent with the prevailing model for how severe convective storm environments are generated (Figure 1).

1) THERMODYNAMIC PROFILE

A schematic of the model thermodynamic profile is shown in Figure 3a. We model the thermodynamic state

identically to AE17 described above, but with three additional useful modifications to put the model into practice.

1. We relax the assumption of constant dry static energy in the free troposphere (i.e. dry adiabatic lapse rate Γ_d) to allow for a constant rate of increase of dry static energy with altitude, β_{FT} . β_{FT} sets the free-tropospheric lapse rate, given by $\Gamma_{FT} = \Gamma_d - \frac{\beta_{FT}}{C_p}$. This is important given that free-tropospheric lapse rates are known to vary significantly in SCS environments (Blanchard 1998); true elevated mixed layers with dry-adiabatic lapse rates are not common through the depth of the troposphere.
2. Since AE17 does not specify a tropopause, we place a simple dry isothermal “stratosphere” layer with temperature T_{TPP} (Chavas and Emanuel 2014) at the model top whose base altitude, H_{TPP} , represents the tropopause altitude. H_{TPP} is defined simply by the height at which the environmental temperature profile equals the tropopause temperature T_{TPP} . This temperature-based definition is desirable given that the tropopause temperature is expected to remain fixed locally with warming in both the tropics and midlatitudes (Seeley et al. 2019; Hartmann and Larson 2002; Thompson et al. 2019).
3. Since AE17 does not specify moisture in the free tropospheric layer, we incorporate the simplest option: constant relative humidity, $RH_{FT}(z) = RH_{FT,0}$. Discussion of additional complexities that could be incorporated are discussed below.

These modifications enable a more realistic representation of historical case soundings and also provide a direct means for testing variations in the thermodynamic profile at fixed CAPE as shown below. One experimental benefit of assuming constant BL dry and moist static energy is that CAPE is then insensitive to the parcel level of origin within the boundary layer (this would not be true for MLCAPe if defined for a layer extending above the boundary layer top). Additional types of complexities that could possibly be added, such as allowing for variations in boundary layer moisture, are discussed below.

2) KINEMATIC PROFILE

A schematic of the model kinematic profile is shown in Figure 3b. We propose a similar two-layer model for representing the kinematic structure of the sounding that is physically consistent with the thermodynamic model. Our model is similar to recent work idealizing the kinematic sounding using L-shaped hodographs that are often seen in tornadic supercell environments (Esterheld and Giuliano 2008; Beck and Weiss 2013; Sherburn and Parker 2015; Guarriello et al. 2018). The model is comprised of a shallow free-tropospheric layer superimposed over a boundary

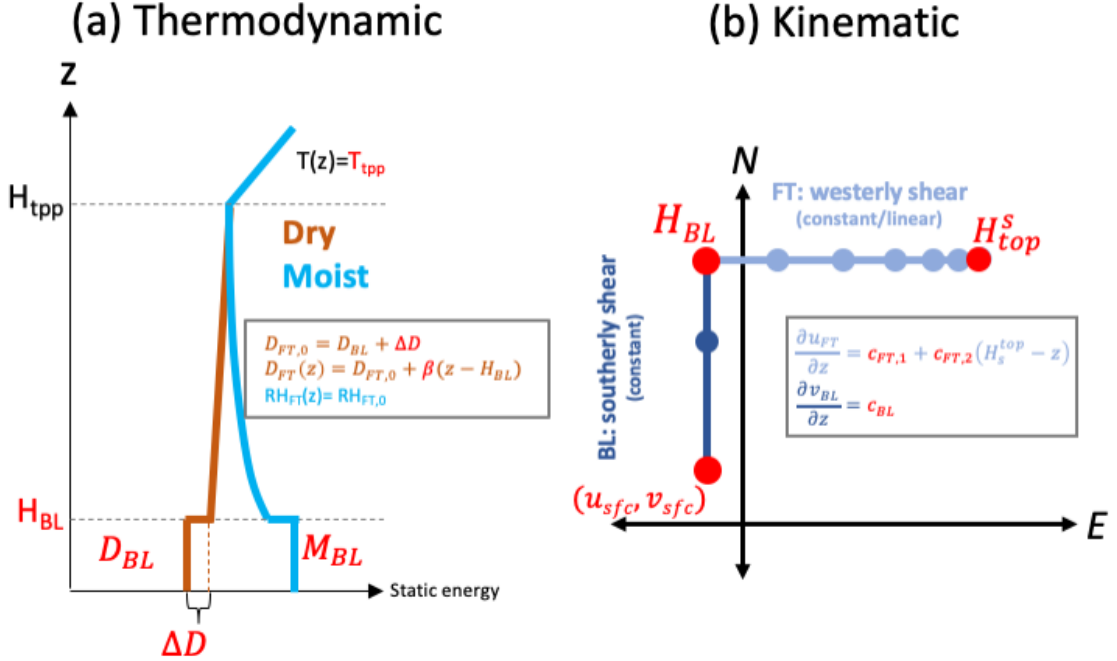


FIG. 3: Schematic of two-layer model for (a) thermodynamic profile, and (b) shear profile. External parameters are colored red. The thermodynamic profile is an extension of the AE17 model. The kinematic model assumes constant southerly shear in the boundary-layer, constant/quadratic westerly shear in the free troposphere, and sets the boundary layer height equal to its value in the thermodynamic profile.

layer with the same depth as the thermodynamic model (H_{BL}). Each layer is assumed to have unidirectional shear, with the boundary layer defined relative to a specified surface wind, (u_{sfc}, v_{sfc}) .

The boundary shear layer is specified with constant southerly shear, i.e.

$$\frac{\partial u_{BL}}{\partial z} = 0 \quad (17)$$

$$\frac{\partial v_{BL}}{\partial z} = c_{BL} \quad (18)$$

c_{BL} represents the constant meridional shear magnitude in the boundary layer. The bulk vector shear across the boundary layer is thus:

$$\Delta V_{BL} = \int_0^{H_{BL}} \frac{\partial v_{BL}}{\partial z} dz = c_{BL} H_{BL} \quad (19)$$

The upper shear layer extends from the base of the free troposphere up to a fixed altitude, H_{top}^s (e.g. on the order of 3-9 km). The layer is specified with westerly shear. We allow this shear to be constant or linearly-decreasing with height, as shear is often concentrated at lower levels in convective storm environments, particularly those associated with tornadic supercells (e.g., Esterheld and Giuliano

2008; Coffey and Parker 2015; Thompson et al. 2003; Coffey et al. 2019), i.e.

$$\frac{\partial u_{FT}}{\partial z} = c_{FT,1} + c_{FT,2}(H_{top}^s - z) \quad (20)$$

$$\frac{\partial v_{FT}}{\partial z} = 0 \quad (21)$$

$c_{FT,2}$ represents the rate of decrease of shear with height. The bulk vector shear across the upper shear layer is thus:

$$\Delta V_{FT} = \int_{H_{BL}}^{H_{top}^s} \frac{\partial u_{FT}}{\partial z} dz = c_{FT,1}(H_{top}^s - H_{BL}) - \frac{1}{2} c_{FT,2}(H_{top}^s - H_{BL})^2 \quad (22)$$

Thus for fixed bulk layer shear, a range of combinations of (c_1, c_2) are possible. There are two simple limit cases to consider for the upper shear layer:

1. Constant shear: $c_{FT,2} = 0$; $c_{FT,1}$ represents the constant zonal shear magnitude
2. Pure linearly-varying shear: $c_{FT,1} = 0$; shear magnitude decreases linearly to zero at $z = H_{top}^s$

For the remainder of the shear profile ($z > H_{top}^s$), we impose zero shear (i.e. constant wind vector).

d. Practical implementation of model

Our objective is to use the model sounding in numerical simulations. We define our model moving upwards from the surface, similar to how a sounding is obtained by an ascending radiosonde. We use Eqs. (1) and (2), the relation between mixing ratio and relative humidity given by $r = \varepsilon \frac{RH e^*}{p - RH e^*}$, where e^* is the saturation vapor pressure. Pressure at each level is calculated iteratively moving upwards assuming hydrostatic balance.

1) THERMODYNAMIC PROFILE

The most straightforward implementation of the thermodynamic model is as follows:

1. Calculate surface dry and moist static energy, D_{sfc} and M_{sfc} , from input surface pressure, temperature, and relative humidity ($P_{sfc}, T_{sfc}, RH_{sfc}$).
2. Calculate boundary layer ($z \leq H_{BL}$) temperature, mixing ratio and pressure assuming constant dry and moist static energy, i.e. $D_{BL} = D_{sfc}$ and $M_{BL} = M_{sfc}$. Mixing ratios are capped such that relative humidity does not exceed 99% (note: this is performed in the final step and thus reduces M_{BL} at those levels).
3. Calculate dry static energy at the base of the FT, defined as the first level above H_{BL} : $D(H_{BL}^+) = D(H_{BL}) + \Delta D$
4. Calculate dry static energy throughout the FT ($z > H_0$): $D_{FT}(z) = D(H_{BL}^+) + \beta_{FT} z$. This quantity defines the free-tropospheric lapse rate, $\Gamma_{FT} = \Gamma_d - \frac{\beta_{FT}}{C_p}$.
5. Calculate free troposphere temperature from $D_{FT}(z)$.
6. Integrate upwards from surface to calculate moisture and hydrostatic pressure at all altitudes, using input free-tropospheric relative humidity ($RH_{FT,0}$).
7. Impose a dry isothermal stratospheric (i.e. statically-stable) layer. This is done by setting the temperature to T_{ipp} and the mixing ratio to 0 at all levels where the predicted free-tropospheric temperature from the previous step is less than the tropopause temperature, $T < T_{ipp}$.

This algorithm specifies the thermodynamic model from the following eight external parameters: $P_{sfc}, T_{sfc}, RH_{sfc}, H_{BL}, \Delta D, T_{ipp}, \Gamma_{FT}$, and $RH_{FT,0}$.

2) KINEMATIC PROFILE

The shear profile may be similarly defined moving upwards from the surface:

1. Define the input surface wind vector, (u_{sfc}, v_{sfc}) .

2. Calculate the boundary shear layer flow velocities ($z \leq H_{BL}$): $u_{BL} = u_{sfc}$, $v_{BL} = v_{sfc} + c_{BL} z$, where c_{BL} represents the average bulk shear in the boundary layer.
3. Calculate the upper shear layer flow velocities ($H_{BL} < z \leq H_{top}^s$): $u_{FT} = u_{BL}(H_{BL}) + c_{FT,1}(H_{top}^s - z) + c_{FT,2}(H_{top}^s - z)^2$, $v_{BL} = v_{BL}(H_{BL})$.
4. Set flow velocities constant for $z > H_{top}^s$

This algorithm specifies the kinematic model from the following six external parameters: $u_{sfc}, v_{sfc}, c_{BL}, c_{FT,1}, c_{FT,2}$, and H_{top}^s . H_{BL} is defined in the thermodynamic model.

3) ADDITIONAL POTENTIAL MODIFICATIONS

The above is a minimal theoretical model that contains the necessary ingredients for a viable environmental SCS sounding. We also incorporated a few additional types of complexity to better capture real-world soundings.

Without question, there are numerous additional degrees of complexity that could be readily added to the model to test their significance. We highlight a few possible options here:

- A water vapor lapse rate within the boundary layer at constant moist static energy. This relaxes the assumption of constant mixing ratio in the boundary layer to parameterize the effects of downward detrainment of dry air across the top of the boundary layer and for surface fluxes of water vapor. The result would be a drying and slight warming near the top of the boundary layer and/or moistening near the surface, but does not otherwise alter the solution. However it does introduce new variation in CAPE and CIN calculated for parcels from different levels (or vertically-averaged) within the BL.
- A water vapor lapse rate at base of free troposphere, to allow for a more gradual moisture transition across the capping inversion. In our model, this transition is sharp.
- Multiple free-tropospheric layers. For example, here we have allowed free tropospheric moisture to vary independently of temperature (dry static energy), which is not characteristic of a true EML. A real EML would also have constant mixing ratio, since the EML was once a well-mixed boundary layer itself. Such a layer could be applied as an intermediate layer in the lower free-troposphere, with constant relative humidity above.
- Height dependence of shear in the boundary layer. Recent studies have found evidence that strong shear in the lowest few hundred m AGL is more closely

related to significant tornado occurrence in supercell storms than the 0-1 km layer more commonly utilized in operational contexts (Markowski et al. 2003; Esterheld and Giuliano 2008; Coffey et al. 2019).

4. Application to historical case: the 3 May 1999 tornado outbreak

a. Fitting the model sounding

We next provide a demonstration of how our model may be used to idealize an SCS environmental sounding associated with a real historical case. We fit our model to a sounding associated with the May 3 1999 tornado outbreak (3MAY99), shown in Figure 2. This sounding successfully produces a long-lived supercell in a 250-m numerical simulation, as will be shown in the Section 4b below.

We fit our model thermodynamic profile to the sounding as follows:

- Set P_{sfc} , T_{sfc} , RH_{sfc} equal to the observed values.
- Set H_{BL} equal to the level of maximum RH
- Set ΔD equal to the difference between the mean DSE in $z \in [H_{BL}, 3H_{BL}]$ and the mean DSE in $z < H_{BL}$. This captures the enhanced dry static energy at the base of the free troposphere.
- Set T_{lpp} equal to the coldest temperature in the sounding, whose altitude defines H_{lpp} .
- Set Γ_{FT} equal to the mean lapse rate in the layer $z \in [H_{BL}, 0.75(H_{BL} + H_{lpp})]$. This average avoids the top of the troposphere where lapse rates necessarily become more stable as they approach the tropopause.
- Set $RH_{FT,0}$ equal to the free-tropospheric column saturation fraction, $\frac{W}{W^*}$. $W = \int_{z_{bot}}^{z_{top}} \rho q_v dz'$ is the actual water vapor path and $W^* = \frac{1}{g} \int_{P_{bot}}^{P_{top}} q_v dP'$ is the actual water vapor path and W^* is its saturation value (Bretherton et al. 2004; Camargo et al. 2014; Raymond et al. 2007). Each term is calculated within the free-tropospheric layer $z \in (H_{BL}, H_{lpp})$. This quantity is effectively identical to a mass-weighted relative humidity (see Appendix), and hence is also commonly called column relative humidity. This approach nearly conserves total layer moisture in the real sounding and thus avoids the addition of significant artificial sources or sinks of latent heat into the column.

This algorithm will yield similar values of surface-based (SB) CAPE.

We fit our model kinematic profile to the sounding as follows:

- Set (u_{sfc}, v_{sfc}) equal to the observed values.

- Set $c_{BL} = \left| \frac{\partial \mathbf{V}_{BL}}{\partial z} \right|$ equal to the average bulk vector shear magnitude in $z < H_{BL}$. This matches the bulk total shear magnitude between the surface and top of the boundary layer and distributes this shear purely in the meridional direction.
- Set H_{top}^s to 3 km. This focuses on the low-level shear.
- Set $c_{FT,1} = 0$ and $c_{FT,2} = -\frac{2}{H_{top}^s - H_{BL}} \left| \frac{\partial \mathbf{V}_{FT}}{\partial z} \right|$, where $\left| \frac{\partial \mathbf{V}_{FT}}{\partial z} \right|$ equals the average bulk vector shear magnitude in $H_{BL} < z < H_{top}^s$. This matches the bulk total shear magnitude between the base and the top of the upper shear layer and distributes this shear purely in the zonal direction. Given that the shear is concentrated at lower levels, we impose a shear profile that linearly decreases to zero at H_{top}^s .

This algorithm also matches the total bulk shear in the sounding across *both* layers ($z < H_{top}^s$). One potential additional kinematic constraint would be to fit the shear profile to the storm-relative helicity. However, this requires precise knowledge of the storm-motion vector, which is a complex function of both the wind profile and internal storm processes such as cold pool propagation (e.g., Bunkers 2018). Nonetheless, we think this could be a valuable addition that we leave for future work.

Our approach is certainly not the only way to fit the model parameters. Here we follow perhaps the most straightforward method to demonstrate how it can be used in practice. We then explore two key sensitivities to illustrate the potential utility of this model to test the importance of key features in the sounding.

Figure 4 displays the theoretical sounding (red, THEO) fit to our example historical event sounding (blue, 3MAY99) following the algorithm described above. For the THEO thermodynamic profile (Figure 4b), the boundary layer dry and moist static energies equal their respective 3MAY99 near-surface values. In the free troposphere, the dry static energy jump is $\Delta D = 2.095 \text{ kJ/kg}$; the relative humidity is $RH_{FT,0} = 0.54$; the lapse rate $\Gamma_{FT} = 7.34 \text{ K/km}$; and the tropopause temperature is $T_{lpp} = 211.25 \text{ K}$. For the THEO kinematic profile (Figure 4c), the surface flow vector equals the 3MAY99 value; and the shear profile constants are $c_{BL} = 0.0293 \text{ s}^{-1}$, $c_{FT,1} = 0$, and $c_{FT,2} = 5.367 \times 10^{-6} \text{ m}^{-1} \text{ s}^{-1}$. Both soundings have similar surface-based CAPE: 4711 J kg^{-1} for 3MAY99 and 4490 J kg^{-1} for THEO. Both soundings have identical 0-3 km bulk shear of 21 ms^{-1} .

To compare the profiles in terms of standard meteorological variables, Figure 4d-f compare temperature, mixing ratio, and relative humidity between THEO and 3MAY99. The temperature structure is remarkably similar at all levels except near the top of the boundary layer where THEO has a sharper capping inversion, indicating

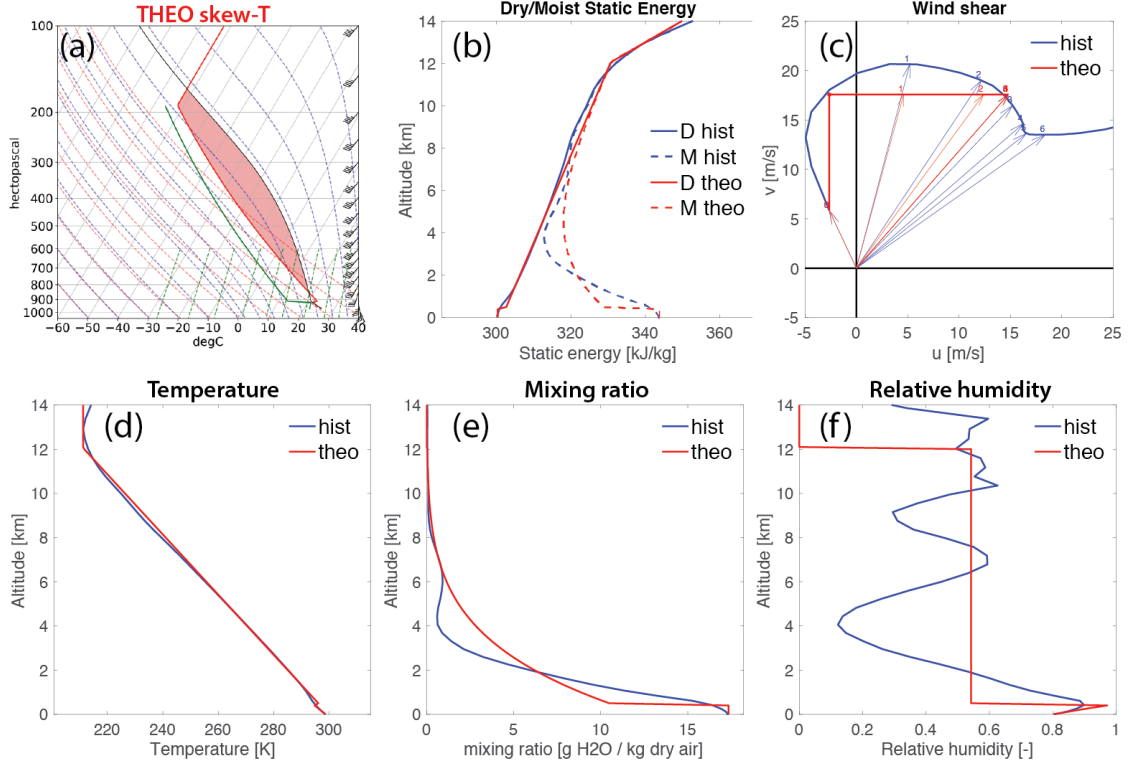


FIG. 4: Comparison of soundings for 3MAY99 historical event (blue) and THEO (red). (a) THEO Skew-T; (b) dry and moist static energies; (c) wind shear; (d) temperature; (e) mixing ratio; (f) relative humidity. Both soundings have similar surface-based CAPE (3MAY99: 4711 J kg^{-1} ; THEO: 4490 J kg^{-1}) and identical 0-3 km bulk shear (21 ms^{-1}).

that in this case the use of a single free-tropospheric lapse rate is quite reasonable. Meanwhile, clearly there are significant vertical variations in free-tropospheric moisture in 3MAY99 that are not represented in our simple model, including greater moisture in the lower free-troposphere and less moisture in the middle free-troposphere. The role of these detailed variations could be tested in future experiments.

b. SCS simulation experiments

Using the experimental setup described in Section 2c, a numerical simulation experiment using the 3MAY99 sounding (Fig. 2) yields a long-lived supercell. Figure 5a displays time series of domain maximum vertical velocity and maximum vertical vorticity at 3km AGL and snapshots of surface simulated radar reflectivity at 1, 2, and 3 h into the simulation.

We next perform a simulation experiment using the theoretical sounding (THEO) and compare against 3MAY99 in Figure 5b. While 3MAY99 produces a long-lived supercell after the initial spin-up period, THEO yields a short-lived convective cell that quickly dissipates after 1 hour despite having environments with similar SBCAPE and bulk shear.

We next perform two demonstration experiments in which we modify our THEO sounding to illustrate the experimental utility of our model.

The sounding used in the first experiment (MODHIST) is “semi-theoretical” in that it is identical to THEO but in which r_v is forced to match 3MAY99 in the lowest 0.84 km (i.e. $2H_{BL}$). Thus it demonstrates how specific details of a real-data sounding may be incorporated into the model to test its importance. The result is shown in Figure 6a. The experiment with this slight modification now produces a long-lived supercell. Owing to both the shallower moisture and the sharper cap in THEO, the SBCIN is -25 J kg^{-1} as compared with -6 J kg^{-1} for 3MAY99. Moreover, the 100-mb mixed-layer (ML) CAPE and CIN for THEO is 2447 J kg^{-1} and -47 J kg^{-1} , respectively, as compared with 3852 J kg^{-1} and -6 J kg^{-1} for 3MAY99. By replacing the THEO low-level moisture profile with that in 3MAY99 for experiment MODHIST, the MLCAP increases to 3552 J kg^{-1} and the MLCIN decreases to -15 J kg^{-1} , while the SBCAPE and SBCIN are very similar to 3MAY99.

The next experiment (MODTHEO) is “fully-theoretical” and demonstrates how physical parameters in the theoretical model can be directly varied to test their importance. Experiment MODTHEO is identical to THEO but with the free-tropospheric relative humidity,

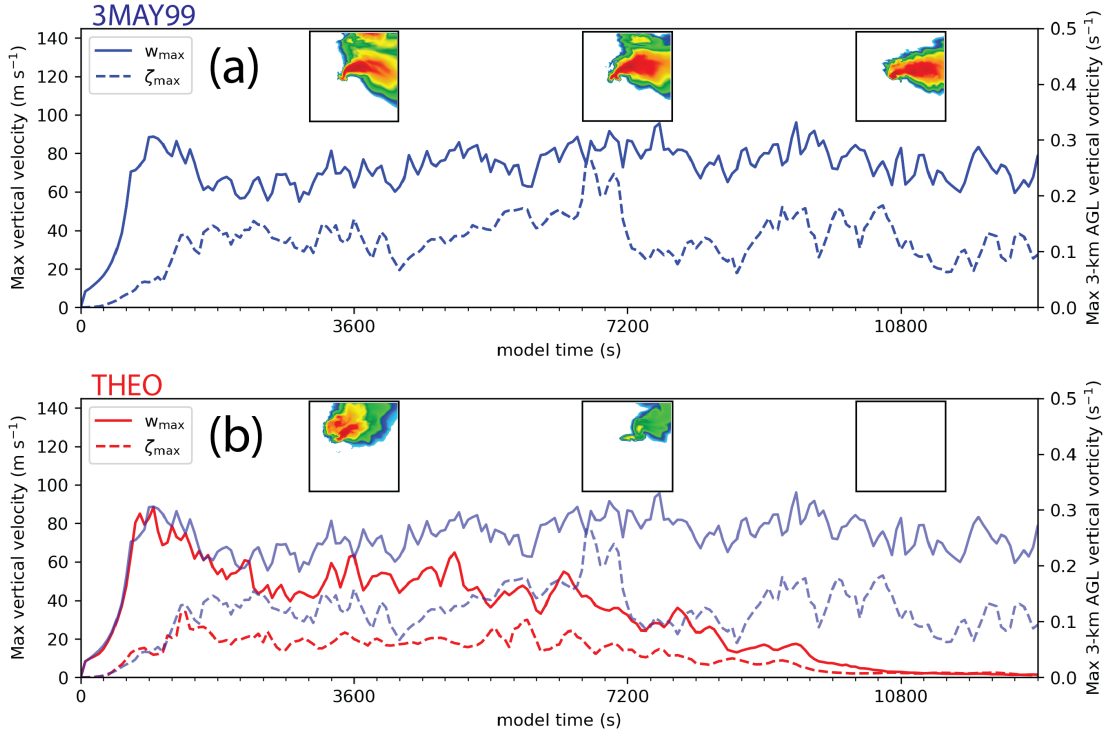


FIG. 5: Simulated supercell evolution associated with (a) historical-event sounding (3MAY99) shown in Figure 2 from the 3 May 1999 tornado outbreak; (b) theoretical sounding (THEO; red) fit to the 3MAY99 sounding, with 3MAY99 result (blue) repeated for comparison. Timeseries show peak vertical velocity (solid) and 3km AGL vertical vorticity (dash) at 3 km AGL, with snapshots of reflectivity (dBz, boxes).

$RH_{FT,0}$, enhanced to 70%. The result is shown in Figure 6b. This experiment also produces a long-lived supercell, similar to both 3MAY99 and MODHIST. Despite having the same BL structure as THEO, the increase in free-tropospheric moisture causes the MLCAPE to increase to 3370 J kg^{-1} and the MLCIN to decrease to -19 J kg^{-1} . Thus, one explanation for the failure to produce a long-lived supercell in THEO is that at least some updraft source parcels for the simulated storm are coming from above the boundary layer, where the air is simply too dry and stable in THEO, such that they dilute the unstable parcels coming from within the boundary layer. This is in keeping with the lower magnitude of MLCAPE and higher magnitude of MLCIN in THEO. Additionally, the greater free-tropospheric moisture in MODTHEO may result in less dilution of updraft parcels throughout their ascent such that they realize more of their CAPE, which is consistent with the findings of James and Markowski (2010).

Thus, taken together, the results of our experiments suggest a substantial sensitivity of convective evolution to the vertical structure of moisture in both the BL and FT. They are consistent with many past studies that highlight the important role of variability in vertical environmental structure in governing storm dynamics (e.g., McCaul Jr and Weisman 2001; McCaul and Cohen 2002; McCaul et al.

2005; Cohen and McCaul 2007; Kirkpatrick et al. 2009; James and Markowski 2010; Dawson et al. 2012; Guarriello et al. 2018; Brown and Nowotarski 2019). However, our experiments are *not* intended to demarcate robust sensitivities. Such an approach would require in-depth experimentation via experimental ensembles and consideration of a range of soundings, whether historical or fully-idealized, which lies beyond the scope of this work. Here we focus simply on presenting the model construction and demonstrating how it could be used to improve our understanding of the effects of any type of variability in a sounding in a simplified setting.

5. Conclusions

Severe convective storm activity depends not only on bulk parameters such as CAPE and lower-tropospheric shear but also on the detailed vertical structure of the thermodynamic and kinematic profiles that can vary independently of those bulk parameters. Past modeling work has tested these dependencies using idealized environmental soundings whose structure and variability is defined empirically rather than physically. A physical model based on the physics of how these environments are generated within the climate system would help to test the role of key details within complex real-data soundings and to link

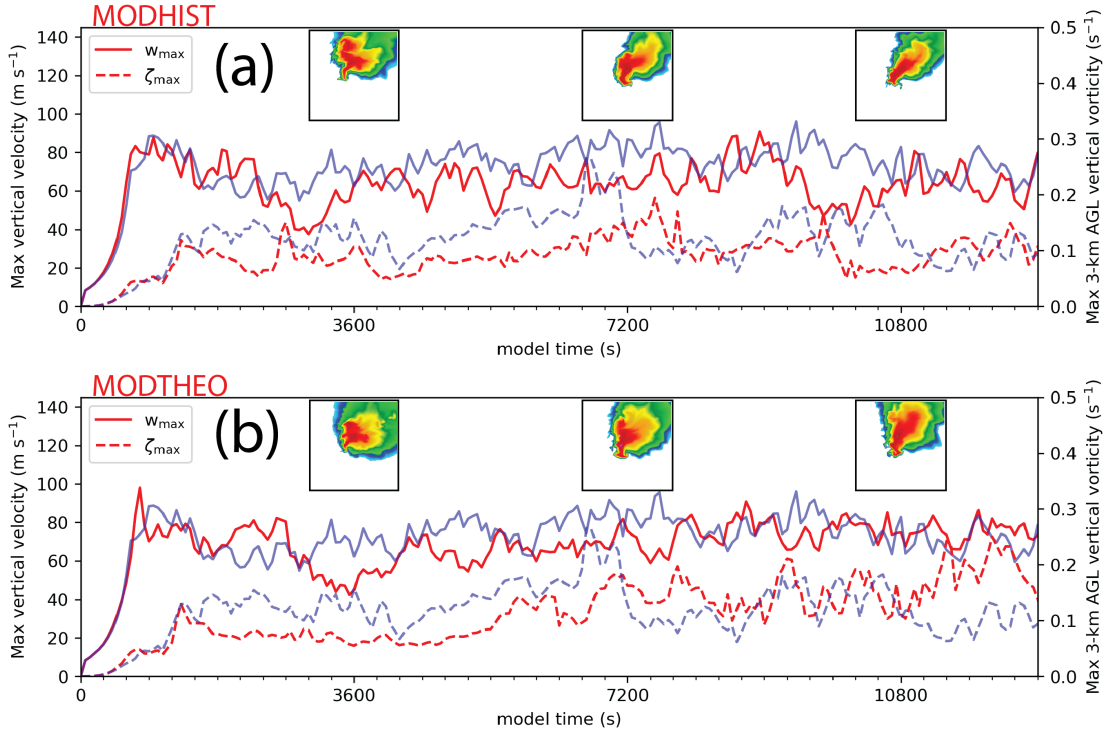


FIG. 6: Simulated supercell evolution for two experiments modifying THEO. (a) MODHIST (red), whose sounding is identical to that of THEO except with r_v forced to match 3MAY99 in the lowest 0.84 km; a long-lived supercell now emerges as was found with 3MAY99. (b) MODTHEO (red), whose sounding is identical to that of THEO except with $RH_{FT,0}$ enhanced to 70%. 3MAY99 evolution also shown (blue). Plot aesthetics as in Figure 5b.

variability in the vertical structure of soundings to the larger-scale climate processes that produce them.

Here we have presented a simple two-layer physical model for the combined steady thermodynamic and kinematic environmental profiles for practical application to the study of severe convective storms. The thermodynamic component of the model builds off of the static energy framework proposed by Agard and Emanuel (2017). The model superposes a boundary layer with constant moist and dry static energy and constant southerly shear beneath a free tropospheric layer with dry static energy increasing linearly with height (allowing a sub-dry-adiabatic lapse rate), constant relative humidity, and westerly shear decreasing linearly to zero. A step-function increase in dry static energy, which represents a capping inversion that scales with convective inhibition, is imposed across the boundary layer top. The model is topped off with a dry isothermal stratosphere that defines the tropopause temperature. Overall, the thermodynamic and kinematic components are mutually consistent, as they represent a transition from predominantly southerly flow advecting warm moist (i.e. high moist static energy) air near the surface to predominantly westerly flow advecting warmer, dry (i.e. high dry static energy) air aloft.

We then provided an algorithm for fitting this theoretical model to a real-data sounding associated with the 3

May 1999 Oklahoma tornado outbreak. Using numerical simulation experiments, we simulated a long-lived supercell with this sounding but only a short-lived storm using the pure theoretical sounding. We then demonstrate two specific types of experiments with our theoretical model that also simulate a long-lived supercell: 1) experiments using semi-theoretical soundings that test the importance of specific features in real soundings by incorporating them directly into the model (here we matched the low-level moisture); and 2) experiments using fully-theoretical soundings that test direct variations in the model's physical parameters (here we enhanced the free-tropospheric relative humidity). These two types of experiments demonstrate the potential utility of our theoretical model to test how SCS evolution depends on the vertical structure of a sounding.

This work has focused simply on presenting for the community the motivation for the model, how the model is constructed, and how it can be applied to a real-data sounding for sensitivity testing and controlled experimentation. The specific outcomes of our simulation examples shown here are *not* intended to demonstrate robust sensitivities. Such tests of any individual parameter or structural feature requires careful experimentation accounting for key sensitivities in model design via ensemble simulations to ensure real, systematic variability. This type of

effort warrants its own separate study, which we hope will be the subject of future research.

Importantly, the specific construction of our theoretical model as presented here should not be interpreted as final – additional details of real soundings not included in the model may yet be of first-order importance for severe convective storm behavior. Instead, this framework should be viewed as a flexible minimal model for an SCS environment amenable to testing but that can readily have structural features added or modified as needed, i.e. there is no single “correct” model. Indeed, we hope that future research testing the model and modifications to it may identify other features that are essential to SCS morphology and evolution and thus should be incorporated into this minimal model for practical applications to understanding the diverse range of SCS types on Earth. Moreover, we note that this modeling framework may potentially be adaptable to other types of convective scenarios, such as nocturnal convection.

Finally, this model may provide an important foundation for linking specific features or types of variability in the vertical structure of an SCS sounding (e.g. free-tropospheric lapse rate) to climate-scale processes that generate them. This will help us to move beyond a focus simply on how bulk parameters such as CAPE may change in a future climate state to further account for how the vertical sounding structure at fixed bulk parameter values may change. The latter is necessary to understand climate change impacts on SCS activity itself and its associated hazards.

References

- Agard, V., and K. Emanuel, 2017: Clausius–clapeyron scaling of peak cape in continental convective storm environments. *Journal of the Atmospheric Sciences*, **74** (9), 3043–3054.
- Agee, E., J. Larson, S. Childs, and A. Marmo, 2016: Spatial redistribution of us tornado activity between 1954 and 2013. *Journal of Applied Meteorology and Climatology*, **55** (8), 1681–1697.
- Beck, J. R., and C. C. Weiss, 2013: An Assessment of Low-Level Baroclinity and Vorticity within a Simulated Supercell. *Monthly Weather Review*, **141** (2), 649–669, doi:10.1175/MWR-D-11-00115.1, URL <http://journals.ametsoc.org/doi/abs/10.1175/MWR-D-11-00115.1>.
- Benjamin, S. G., 1986: Some effects of surface heating and topography on the regional severe storm environment. part ii: Two-dimensional idealized experiments. *Monthly weather review*, **114** (2), 330–343.
- Benjamin, S. G., and T. N. Carlson, 1986: Some effects of surface heating and topography on the regional severe storm environment. part i: Three-dimensional simulations. *Monthly Weather Review*, **114** (2), 307–329.
- Blanchard, D. O., 1998: Assessing the vertical distribution of convective available potential energy. *Weather and Forecasting*, **13** (3), 870–877.
- Bretherton, C. S., M. E. Peters, and L. E. Back, 2004: Relationships between water vapor path and precipitation over the tropical oceans. *Journal of climate*, **17** (7), 1517–1528.
- Brooks, H. E., C. A. Doswell, and J. Cooper, 1994: On the Environments of Tornadic and Nontornadic Mesocyclones. URL [http://journals.ametsoc.org/doi/abs/10.1175/1520-0434\(1994\)009%3C0606:OTEOTA%3E2.0.CO;2](http://journals.ametsoc.org/doi/abs/10.1175/1520-0434(1994)009%3C0606:OTEOTA%3E2.0.CO;2), 606–618 pp., doi:[http://dx.doi.org/10.1175/1520-0434\(1994\)009%3C0606:OTEOTA%3E2.0.CO;2](http://dx.doi.org/10.1175/1520-0434(1994)009%3C0606:OTEOTA%3E2.0.CO;2).
- Brooks, H. E., J. W. Lee, and J. P. Craven, 2003: The spatial distribution of severe thunderstorm and tornado environments from global reanalysis data. *Atmospheric Research*, **67**, 73–94.
- Brown, M., and C. J. Nowotarski, 2019: The influence of lifting condensation level on low-level outflow and rotation in simulated supercell thunderstorms. *Journal of the Atmospheric Sciences*, **76** (5), 1349–1372, doi:10.1175/JAS-D-18-0216.1, URL <https://doi.org/10.1175/JAS-D-18-0216.1>, <https://doi.org/10.1175/JAS-D-18-0216.1>.
- Bryan, G. H., 2008: On the computation of pseudoadiabatic entropy and equivalent potential temperature. *Monthly Weather Review*, **136** (12), 5239–5245.
- Bryan, G. H., and J. M. Fritsch, 2002: A benchmark simulation for moist nonhydrostatic numerical models. *Monthly Weather Review*, **130** (12), 2917–2928.
- Bryan, G. H., J. C. Knievel, and M. D. Parker, 2006: A Multi-model Assessment of RKW Theorys Relevance to Squall-Line Characteristics. *Monthly Weather Review*, **134** (10), 2772–2792, doi:10.1175/MWR3226.1, URL <http://journals.ametsoc.org/doi/abs/10.1175/MWR3226.1> <http://ams.allenpress.com/perlserv/?request=get-abstract&doi=10.1175/MWR3226.1> http://www.ral.ucar.edu/staff/knievel/pubs/bryan_et_al_mwr_2006.pdf.
- Bryan, G. H., and R. Rotunno, 2009: Evaluation of an analytical model for the maximum intensity of tropical cyclones. *Journal of the Atmospheric Sciences*, **66** (10), 3042–3060.
- Bu, Y. P., R. G. Fovell, and K. L. Corbosiero, 2014: Influence of cloud-radiative forcing on tropical cyclone structure. *Journal of the Atmospheric Sciences*, **71** (5), 1644–1662.
- Bunkers, M. J., 2018: Observations of right-moving supercell motion forecast errors. *Weather and Forecasting*, **33** (1), 145–159, doi:10.1175/WAF-D-17-0133.1.
- Camargo, S. J., M. K. Tippett, A. H. Sobel, G. A. Vecchi, and M. Zhao, 2014: Testing the performance of tropical cyclone genesis indices in future climates using the HIRAM model. *Journal of Climate*, **27** (24), 9171–9196.
- Carlson, T., and F. Ludlam, 1968: Conditions for the occurrence of severe local storms. *Tellus*, **20** (2), 203–226.
- Chavas, D. R., and K. Emanuel, 2014: Equilibrium tropical cyclone size in an idealized state of axisymmetric radiative–convective equilibrium*. *Journal of the Atmospheric Sciences*, **71** (5), 1663–1680.
- Cintineo, R. M., and D. J. Stensrud, 2013: On the Predictability of Supercell Thunderstorm Evolution. *Journal of the Atmospheric Sciences*, **70** (7), 1993–2011, doi:10.1175/JAS-D-12-0166.1, URL <http://journals.ametsoc.org/doi/abs/10.1175/JAS-D-12-0166.1>.
- Coffer, B. E., and M. D. Parker, 2015: Impacts of Increasing Low-Level Shear on Supercells during the Early Evening Transition. *Monthly Weather Review*, **143** (5), 1945–1969, doi:10.1175/MWR-D-14-00328.1, URL <http://journals.ametsoc.org/doi/10.1175/MWR-D-14-00328.1>.
- Coffer, B. E., M. D. Parker, R. L. Thompson, B. T. Smith, and R. E. Jewell, 2019: Using near-ground storm relative helicity in supercell

- tornado forecasting. *Weather and Forecasting*, **34** (5), 1417–1435, doi:10.1175/WAF-D-19-0115.1.
- Cohen, C., and E. W. McCaul, 2007: Further results on the sensitivity of simulated storm precipitation efficiency to environmental temperature. *Monthly Weather Review*, **135** (5), 1671–1684, doi:10.1175/MWR3380.1.
- Dahl, J. M. L., 2015: Near-Ground Rotation in Simulated Supercells: On the Robustness of the Baroclinic Mechanism. *Monthly Weather Review*, 150914120152001, doi:10.1175/MWR-D-15-0115.1, URL <http://journals.ametsoc.org/doi/abs/10.1175/MWR-D-15-0115.1>.
- Dahl, J. M. L., M. D. Parker, and L. J. Wicker, 2012: Uncertainties in Trajectory Calculations within Near-Surface Mesocyclones of Simulated Supercells. *Monthly Weather Review*, **140** (9), 2959–2966, doi:10.1175/MWR-D-12-00131.1, URL <http://journals.ametsoc.org/doi/abs/10.1175/MWR-D-12-00131.1>.
- Dahl, J. M. L., M. D. Parker, and L. J. Wicker, 2014: Imported and Storm-Generated Near-Ground Vertical Vorticity in a Simulated Supercell. *Journal of the Atmospheric Sciences*, **71**, 3027–3051, doi:10.1175/JAS-D-13-0123.1, URL <http://journals.ametsoc.org/doi/abs/10.1175/JAS-D-13-0123.1>.
- Davenport, C. E., and M. D. Parker, 2015: Impact of environmental heterogeneity on the dynamics of a dissipating supercell thunderstorm. *Monthly Weather Review*, **143** (10), 4244–4277, doi:10.1175/MWR-D-15-0072.1.
- Davis, C. A., 2015: The formation of moist vortices and tropical cyclones in idealized simulations. *Journal of the Atmospheric Sciences*, (2015).
- Dawson, D. T., E. R. Mansell, Y. Jung, L. J. Wicker, M. R. Kumjian, and M. Xue, 2014: Low-level ZDR signatures in supercell forward flanks: The role of size sorting and melting of hail. *Journal of the Atmospheric Sciences*, **71** (1), 276–299, doi:10.1175/JAS-D-13-0118.1.
- Dawson, D. T., B. Roberts, and M. Xue, 2019: A method to control the environmental wind profile in idealized simulations of deep convection with surface friction. *Monthly Weather Review*, Early online release, doi:10.1175/mwr-d-18-0462.1.
- Dawson, D. T., L. J. Wicker, E. R. Mansell, and R. L. Tanamachi, 2012: Impact of the environmental low-level wind profile on ensemble forecasts of the 4 May 2007 Greensburg, Kansas, tornadic storm and associated mesocyclones. *Monthly Weather Review*, **140** (2), 696–716, doi:10.1175/MWR-D-11-00008.1.
- Dawson, D. T., M. Xue, J. A. Milbrandt, and M. K. Yau, 2010: Comparison of evaporation and cold pool development between single-moment and multimoment bulk microphysics schemes in idealized simulations of tornadic thunderstorms. *Monthly Weather Review*, **138** (4), 1152–1171, doi:10.1175/2009MWR2956.1, URL <http://journals.ametsoc.org/doi/abs/10.1175/2009MWR2956.1>.
- Deardorff, J. W., 1980: Stratocumulus-capped mixed layers derived from a three-dimensional model. *Boundary-Layer Meteorology*, **18** (4), 495–527, doi:10.1007/BF00119502.
- Diffenbaugh, N. S., M. Scherer, and R. J. Trapp, 2013: Robust increases in severe thunderstorm environments in response to greenhouse forcing. *Proceedings of the National Academy of Sciences*, **110** (41), 16 361–16 366.
- Doswell, C. A., 2001: Severe convective storms: an overview. *Severe convective storms*, Springer, 1–26.
- Doswell III, C. A., H. E. Brooks, and R. A. Maddox, 1996: Flash flood forecasting: An ingredients-based methodology. *Weather and Forecasting*, **11** (4), 560–581.
- Duda, J. D., and W. A. Gallus, 2013: The Impact of Large-Scale Forcing on Skill of Simulated Convective Initiation and Up-scale Evolution with Convection-Allowing Grid Spacings in the WRF. *Weather and Forecasting*, **28** (4), 994–1018, doi:10.1175/WAF-D-13-00005.1, URL <http://journals.ametsoc.org/doi/abs/10.1175/WAF-D-13-00005.1>.
- Elmore, K. L., D. J. Stensrud, and K. C. Crawford, 2002a: Ensemble Cloud Model Applications to Forecasting Thunderstorms. *Journal of Applied Meteorology*, **41** (4), 363–383, doi:10.1175/1520-0450(2002)041<0363:ECMATF>2.0.CO;2, URL <http://journals.ametsoc.org/doi/abs/10.1175/1520-0450%282002%29041%3C0363%3AECMATF%3E2.0.CO%3B2>.
- Elmore, K. L., D. J. Stensrud, K. C. Crawford, K. L. Elmore, D. J. Stensrud, and K. C. Crawford, 2002b: Explicit Cloud-Scale Models for Operational Forecasts: A Note of Caution. *Weather and Forecasting*, **17** (4), 873–884, doi:10.1175/1520-0434(2002)017<0873:ECSMFO>2.0.CO;2, URL <http://journals.ametsoc.org/doi/abs/10.1175/1520-0434%282002%29017%3C0873%3AECSMFO%3E2.0.CO%3B2>.
- Emanuel, K., 2004: Tropical cyclone energetics and structure. *Atmospheric turbulence and mesoscale meteorology*, (8), 165–191.
- Esterheld, J. M., and D. J. Giuliano, 2008: Discriminating between Tornadoic and Non-Tornadoic Supercells: A New Hodograph Technique. *E-Journal of Severe Storms Meteorology*, **3** (2), 1–50, URL <http://www.ejssm.org/ojs/index.php/ejssm/article/view/33/37>.
- Gensini, V. A., and W. S. Ashley, 2011: Climatology of potentially severe convective environments from the north american regional reanalysis. *E-Journal of Severe Storms Meteorology*, **6** (8).
- Gensini, V. A., and H. E. Brooks, 2018: Spatial trends in united states tornado frequency. *npj Climate and Atmospheric Science*, **1** (1), 38.
- Gensini, V. A., and T. L. Mote, 2015: Downscaled estimates of late 21st century severe weather from ccs3. *Climatic Change*, **129** (1–2), 307–321.
- Gilmore, M. S., and L. J. Wicker, 1998: The influence of midtropospheric dryness on supercell morphology and evolution. *Monthly Weather Review*, **126** (4), 943–958, doi:10.1175/1520-0493(1998)126<0943:TIOMDO>2.0.CO;2, URL [http://ams.allenpress.com/perlserv/?request=get-abstract&doi=10.1175/1520-0493\(1998\)126%3C0943:TIOMDO%3E2.0.CO;2](http://ams.allenpress.com/perlserv/?request=get-abstract&doi=10.1175/1520-0493(1998)126%3C0943:TIOMDO%3E2.0.CO;2); [http://ams.allenpress.com/amsonline/?request=get-abstract&doi=10.1175/1520-0493\(1998\)126%3C0943:TIOMDO%3E2.0.CO;2](http://ams.allenpress.com/amsonline/?request=get-abstract&doi=10.1175/1520-0493(1998)126%3C0943:TIOMDO%3E2.0.CO;2).
- Guarriello, F., C. J. Nowotarski, and C. C. Epifanio, 2018: Effects of the Low-Level Wind Profile on Outflow Position and Near-Surface Vertical Vorticity in Simulated Supercell Thunderstorms. *Journal of the Atmospheric Sciences*, **75** (3), 731–753, doi:10.1175/jas-d-17-0174.1.
- Hartmann, D. L., and K. Larson, 2002: An important constraint on tropical cloud-climate feedback. *Geophysical Research Letters*, **29** (20), 12–1.
- Honda, T., and T. Kawano, 2015: How does mid-tropospheric dry air affect the evolution of supercellular convection? *Atmospheric Research*, **157**, 1–16, doi:10.1016/j.atmosres.2015.01.015, URL <http://dx.doi.org/10.1016/j.atmosres.2015.01.015>.

- Hoogewind, K. A., M. E. Baldwin, and R. J. Trapp, 2017: The impact of climate change on hazardous convective weather in the united states: insight from high-resolution dynamical downscaling. *Journal of Climate*, **30** (24), 10 081–10 100.
- Hunter, J. D., 2007: Matplotlib: A 2d graphics environment. *Computing in Science & Engineering*, **9** (3), 90–95, doi:10.1109/MCSE.2007.55.
- James, R. P., and P. M. Markowski, 2010: A Numerical Investigation of the Effects of Dry Air Aloft on Deep Convection. *Monthly Weather Review*, **138** (1), 140–161, doi:10.1175/2009MWR3018.1, URL <http://journals.ametsoc.org/doi/abs/10.1175/2009MWR3018.1>.
- Kirkpatrick, C., E. W. McCaul, and C. Cohen, 2009: Variability of Updraft and Downdraft Characteristics in a Large Parameter Space Study of Convective Storms. *Monthly Weather Review*, **137** (5), 1550–1561, doi:10.1175/2008mwr2703.1.
- Lawson, J. R., 2019: Predictability of idealized thunderstorms in buoyancy–shear space. *Journal of the Atmospheric Sciences*, **76** (9), 2653–2672.
- Mansell, E. R., 2010: On Sedimentation and Advection in Multimoment Bulk Microphysics. *Journal of the Atmospheric Sciences*, **67** (9), 3084–3094, doi:10.1175/2010JAS3341.1, URL <http://journals.ametsoc.org/doi/abs/10.1175/2010JAS3341.1>.
- Markowski, P. M., 2016: An idealized numerical simulation investigation of the effects of surface drag on the development of near-surface vertical vorticity in supercell thunderstorms. *Journal of the Atmospheric Sciences*, 16–0150, doi:10.1175/JAS-D-16-0150.1, URL <http://journals.ametsoc.org/doi/10.1175/JAS-D-16-0150.1>.
- Markowski, P. M., C. Hannon, J. Frame, E. Lancaster, A. Pietrycha, R. Edwards, and R. L. Thompson, 2003: Characteristics of Vertical Wind Profiles near Supercells Obtained from the Rapid Update Cycle. *Weather and Forecasting*, **18** (6), 1262–1272, doi:10.1175/1520-0434(2003)018<1262:COVWPN>2.0.CO;2, URL <http://journals.ametsoc.org/doi/abs/10.1175/1520-0434%282003%29018%3C1262%3ACOVWPN%3E2.0.CO%3B2>.
- May, R. M., S. C. Arms, P. Marsh, E. Bruning, J. R. Leeman, K. Goebert, J. E. Thielen, and Z. S. Bruick, 2008–2020: Metpy: A Python package for meteorological data. Boulder, Colorado, URL <https://github.com/Unidata/MetPy>, doi:10.5065/D6WW7G29.
- McCaul, E. W., and C. Cohen, 2002: The impact of simulated storm structure and intensity of variations in the mixed layer and moist layer depths. *Monthly Weather Review*, **130** (7), 1722–1748, doi:10.1175/1520-0493(2002)130<1722:TIOSSS>2.0.CO;2.
- McCaul, E. W., and C. Cohen, 2004: The initiation, longevity and morphology of simulated convective storms as a function of free-tropospheric relative humidity. *22nd Conference on Severe Local Storms*, American Meteorological Society, Hyannis, MA, 8A.5.
- McCaul, E. W., C. Cohen, and C. Kirkpatrick, 2005: The Sensitivity of Simulated Storm Structure, Intensity, and Precipitation Efficiency to Environmental Temperature. *Monthly Weather Review*, **133** (10), 3015–3037, doi:10.1175/MWR3015.1, URL <http://journals.ametsoc.org/doi/abs/10.1175/MWR3015.1>.
- McCaul Jr, E. W., and M. L. Weisman, 2001: The sensitivity of simulated supercell structure and intensity to variations in the shapes of environmental buoyancy and shear profiles. *Monthly Weather Review*, **129** (4), 664–687.
- Navarro, E. L., and G. J. Hakim, 2016: Idealized numerical modeling of the diurnal cycle of tropical cyclones. *Journal of the Atmospheric Sciences*, **73** (10), 4189–4201.
- Naylor, J., and M. S. Gilmore, 2012: Convective Initiation in an Idealized Cloud Model Using an Updraft Nudging Technique. *Monthly Weather Review*, **140** (11), 3699–3705, doi:10.1175/MWR-D-12-00163.1, URL <http://journals.ametsoc.org/doi/abs/10.1175/MWR-D-12-00163.1>.
- Naylor, J., and M. S. Gilmore, 2014: Corrigendum. *Journal of the Atmospheric Sciences*, **71** (9), 3568–3568, doi:10.1175/JAS-D-14-0204.1, URL <http://journals.ametsoc.org/doi/abs/10.1175/JAS-D-14-0204.1>.
- Naylor, J., and D. A. Schecter, 2014: Evaluation of the impact of moist convection on the development of asymmetric inner core instabilities in simulated tropical cyclones. *Journal of Advances in Modeling Earth Systems*, **6** (4), 1027–1048.
- Nowotarski, C. J., and P. M. Markowski, 2016: Modifications to the Near-Storm Environment Induced by Simulated Supercell Thunderstorms. *Monthly Weather Review*, **144** (1), 273–293, doi:10.1175/MWR-D-15-0247.1, URL <http://journals.ametsoc.org/doi/10.1175/MWR-D-15-0247.1>.
- Orf, L., R. B. Wilhelmson, B. Lee, C. A. Finley, and A. Houston, 2017: Evolution of a long-track violent tornado within a simulated supercell. *Bulletin of the American Meteorological Society*, **98** (1), 45–68, doi:10.1175/BAMS-D-15-00073.1, URL <http://journals.ametsoc.org/doi/10.1175/BAMS-D-15-00073.1>.
- Parker, M. D., 2014: Composite VORTEX2 Supercell Environments from Near-Storm Soundings. *Monthly Weather Review*, **142** (2), 508–529, doi:10.1175/MWR-D-13-00167.1, URL <http://journals.ametsoc.org/doi/abs/10.1175/MWR-D-13-00167.1>.
- Peng, K., R. Rotunno, and G. H. Bryan, 2018: Evaluation of a time-dependent model for the intensification of tropical cyclones. *Journal of the Atmospheric Sciences*, **75** (6), 2125–2138.
- Rasmussen, E. N., and D. O. Blanchard, 1998: A Baseline Climatology of Sounding-Derived Supercell and Tornado Forecast Parameters. *Weather and Forecasting*, **13** (4), 1148–1164, doi:10.1175/1520-0434(1998)013<1148:ABCOSD>2.0.CO;2, URL <http://journals.ametsoc.org/doi/abs/10.1175/1520-0434%281998%29013%3C1148%3AABCOSD%3E2.0.CO%3B2>.
- Raymond, D. J., S. L. Sessions, and Ž. Fuchs, 2007: A theory for the spinup of tropical depressions. *Quarterly Journal of the Royal Meteorological Society: A journal of the atmospheric sciences, applied meteorology and physical oceanography*, **133** (628), 1743–1754.
- Romps, D. M., 2015: Mse minus cape is the true conserved variable for an adiabatically lifted parcel. *Journal of the Atmospheric Sciences*, **72** (9), 3639–3646.
- Seeley, J. T., N. Jeevanjee, and D. M. Romps, 2019: Fat or fitt: Are anvil clouds or the tropopause temperature invariant? *Geophysical Research Letters*, **46** (3), 1842–1850.
- Seeley, J. T., and D. M. Romps, 2015: The effect of global warming on severe thunderstorms in the united states. *Journal of Climate*, **28** (6), 2443–2458.
- Sherburn, K. D., and M. D. Parker, 2014: Climatology and Ingredients of Significant Severe Convection in High Shear, Low

- CAPE Environments. *Weather and Forecasting*, **29**, 854–877, doi:10.1175/WAF-D-13-00041.1, URL <http://journals.ametsoc.org/doi/abs/10.1175/WAF-D-13-00041.1>.
- Sherburn, K. D., and M. D. Parker, 2015: Examining the sensitivities of high-shear, low-CAPE convection on low-level hodograph shape. *16th Conference on Mesoscale Processes*, 11.2A.
- Singh, M. S., and P. A. O’Gorman, 2013: Influence of entrainment on the thermal stratification in simulations of radiative-convective equilibrium. *Geophysical Research Letters*, **40** (16), 4398–4403.
- Singh, M. S., and P. A. O’Gorman, 2014: Influence of microphysics on the scaling of precipitation extremes with temperature. *Geophysical Research Letters*, **41** (16), 6037–6044.
- Singh, M. S., and P. A. O’Gorman, 2015: Increases in moist-convective updraught velocities with warming in radiative-convective equilibrium. *Quarterly Journal of the Royal Meteorological Society*, **141** (692), 2828–2838.
- Speheger, D. A., C. A. Doswell, and G. J. Stumpf, 2002: The Tornadoes of 3 May 1999: Event Verification in Central Oklahoma and Related Issues. *Weather and Forecasting*, **17** (3), 362–381, doi:10.1175/1520-0434(2002)017<0362:TTOMEV>2.0.CO;2, URL [http://ams.allenpress.com/perlserv/?request=get-abstract&doi=10.1175/1520-0434\(2002\)017%3C0362:TTOMEV%3E2.0.CO;2http://journals.ametsoc.org/doi/abs/10.1175/1520-0434\(2002\)017%3C0362:TTOMEV%3E2.0.CO;2](http://ams.allenpress.com/perlserv/?request=get-abstract&doi=10.1175/1520-0434(2002)017%3C0362:TTOMEV%3E2.0.CO;2http://journals.ametsoc.org/doi/abs/10.1175/1520-0434(2002)017%3C0362:TTOMEV%3E2.0.CO;2).
- Thompson, D. W., P. Ceppi, and Y. Li, 2019: A robust constraint on the temperature and height of the extratropical tropopause. *Journal of Climate*, **32** (2), 273–287.
- Thompson, R. L., R. Edwards, J. a. Hart, K. L. Elmore, and P. M. Markowski, 2003: Close Proximity Soundings within Supercell Environments Obtained from the Rapid Update Cycle. *Weather and Forecasting*, **18** (6), 1243–1261, doi:10.1175/1520-0434(2003)018<1243:CPSWSE>2.0.CO;2.
- Thompson, R. L., R. Edwards, and C. M. Mead, 2004: An update to the supercell composite and significant tornado parameters. *Preprints, 22nd Conf. on Severe Local Storms, Hyannis, MA, Amer. Meteor. Soc. P.*, Vol. 8.
- Tippett, M. K., J. T. Allen, V. A. Gensini, and H. E. Brooks, 2015: Climate and hazardous convective weather. *Current Climate Change Reports*, **1** (2), 60–73.
- Trapp, R. J., N. S. Diffenbaugh, H. E. Brooks, M. E. Baldwin, E. D. Robinson, and J. S. Pal, 2007: Changes in severe thunderstorm environment frequency during the 21st century caused by anthropogenically enhanced global radiative forcing. *Proceedings of the National Academy of Sciences*, **104** (50), 19719–19723.
- Trapp, R. J., N. S. Diffenbaugh, and A. Gluhovsky, 2009: Transient response of severe thunderstorm forcing to elevated greenhouse gas concentrations. *Geophysical Research Letters*, **36** (1).
- Trapp, R. J., and K. A. Hoogewind, 2016: The realization of extreme tornadic storm events under future anthropogenic climate change. *Journal of Climate*, **29** (14), 5251–5265.
- Trapp, R. J., K. A. Hoogewind, and S. Lasher-Trapp, 2019: Future changes in hail occurrence in the united states determined through convection-permitting dynamical downscaling. *Journal of Climate*, **32** (17), 5493–5509.
- Trapp, R. J., E. D. Robinson, M. E. Baldwin, N. S. Diffenbaugh, and B. R. Schwedler, 2011: Regional climate of hazardous convective weather through high-resolution dynamical downscaling. *Climate dynamics*, **37** (3–4), 677–688.
- Weisman, M. L., and J. B. Klemp, 1982a: The dependence of numerically simulated convective storms on vertical wind shear and buoyancy. *Monthly Weather Review*, **110** (6), 504–520.
- Weisman, M. L., and J. B. Klemp, 1982b: The Dependence of Numerically Simulated Convective Storms on Vertical Wind Shear and Buoyancy. *Monthly Weather Review*, **110** (6), 504–520, doi:10.1175/1520-0493(1982)110<0504:TDONSC>2.0.CO;2, URL [http://journals.ametsoc.org/doi/abs/10.1175/1520-0493\(1982\)110%3C0504:TDONSC%3E2.0.CO;2](http://journals.ametsoc.org/doi/abs/10.1175/1520-0493(1982)110%3C0504:TDONSC%3E2.0.CO;2).
- Weisman, M. L., and J. B. Klemp, 1984a: The structure and classification of numerically simulated convective storms in directionally varying wind shears. *Monthly Weather Review*, **112** (12), 2479–2498.
- Weisman, M. L., and J. B. Klemp, 1984b: The Structure and Classification of Numerically Simulated Convective Storms in Directionally Varying Wind Shears. *Monthly Weather Review*, **112** (12), 2479–2498, doi:10.1175/1520-0493(1984)112<2479:TSACON>2.0.CO;2, URL [http://journals.ametsoc.org/doi/abs/10.1175/1520-0493\(1984\)112%3C2479:TSACON%3E2.0.CO;2http://ams.allenpress.com/perlserv/?request=get-abstract&doi=10.1175/1520-0493\(1984\)112%3C2479:TSACON%3E2.0.CO;2](http://journals.ametsoc.org/doi/abs/10.1175/1520-0493(1984)112%3C2479:TSACON%3E2.0.CO;2http://ams.allenpress.com/perlserv/?request=get-abstract&doi=10.1175/1520-0493(1984)112%3C2479:TSACON%3E2.0.CO;2).

Data Availability Statement

All data and code from this manuscript are available by emailing the corresponding author at drchavas@gmail.com.

Acknowledgments. Chavas was partially supported by NSF grant 1648681 and NOAA grant NA16OAR4590208. Dawson was partially supported by NOAA grants NA16OAR4590208 and NA18OAR4590313. The authors gratefully acknowledge the open-source Python community, and particularly the authors and contributors to the Matplotlib (Hunter 2007) and MetPy (May et al. 2008 - 2020) packages that were used to generate many of the figures. Finally, the authors thank Tim Cronin and Mike Baldwin for useful discussions that helped improve this manuscript.

APPENDIX

Saturation fraction vs. Relative humidity

For Earth-like atmospheres in which the saturation vapor pressure is small compared to the total pressure, i.e. $e^* \ll P$, one can show that the saturation fraction and relative humidity of an air parcel are nearly identical.

Relative humidity is defined as

$$RH = \frac{e}{e^*} \quad (\text{A1})$$

Saturation fraction is defined as

$$SF = \frac{q}{q^*} \quad (\text{A2})$$

These equations may be combined with the relations

$$q = \frac{r}{1+r} \quad (\text{A3})$$

and

$$r = \varepsilon \frac{e}{P-e} \quad (\text{A4})$$

and their saturated counterparts, where $\varepsilon = \frac{R_d}{R_v} = 0.622$ is the ratio of specific gas constants for dry air and water vapor. The result may be written as

$$SF = RH \left(\frac{1 - \frac{(1-\varepsilon)e^*}{P}}{1 - \frac{(1-\varepsilon)e}{P}} \right) \quad (\text{A5})$$

Thus if $(1-\varepsilon)e^* \ll P$, then $SF \approx RH$. This easily holds for the modern Earth atmosphere, for which at very warm temperatures $(1-\varepsilon)e^* \approx (1-0.622)(0.5 \text{ hPa}) \approx 0.2 \text{ hPa}$ which is several orders of magnitude smaller than the associated surface pressures of 1000 hPa. Indeed, the vertical profiles of SF and RH are indistinguishable for the 3MAY99 sounding presented here.